(2)

N00014-85-K-2025

DATE: October 24, 1986

FROM: Dr. S. Suckewer

SUBJECT: Final Progress Report on Princeton University "X-Ray Laser Related Line Identifications of Neon-Like Ions"

TO: Dr. S. Ossakow, Code 4700

ENCL: (1) Two papers by Dr. S. Suckewer et.al.

1. Please find attached two papers done at Princeton by S. Suckewer et.al. and at NRL by Feldman, Seely, and Dave. These two papers report the analysis of high resolution, time resolved spectra from the PLT tokamak plasma. Data was collected on a large number of PLT discharges. The spectra from the highly-charged ions from the wall material (Fe, Ni, Cr, and Ti) were recorded, and spectra from the injected elements, Fe, Ni, Zn, Ge, Se, and Mo were produced using the laser ablation technique. A very precise wavelength scale was established using well-known reference lines. A number of transitions of the type $\Delta n = 0$ and terminating on levels within the ground configurations were identified.

2. The primary purpose was to produce an abundance of Ne-like ions in the PLT discharge and to search for Ne-like transitions of the type 3s-3p. The F-like and Na-like ionization stage was certainly produced. However, the 3s-3p transitions were very weak, and conclusive identifications could not be made. In general, the ground state transitions are intense in the PLT plasma, and transitions between excited states are weaker.

3. It was found that the PLT tokamak with its variety of very sophisticated diagnostic instruments, and with very reproducible and higher temperature plasma, is an extremely good device for spectroscopic and atomic physics studies. PLT suits particularly well for spectral line identifications for X-ray laser research. With recently obtained very high electron temperatures $\sim$ 5-6 keV, using additional RF heating (Lower Hybrid), PLT could be used for observation transitions in very highly ionized high-Z elements necessary for the development of X-ray lasers with a shorter wavelength.

TIME-RESOLVED SPECTRA IN THE 80-340 Å WAVELENGTH REGION FROM PLT TOKAMAK PLASMAS*

J.H. Davé
Applied Research Corporation
8201 Corporate Drive
Landover, MD 20785

U. Feldman and J.F. Seely
E.O. Hulburt Center for Space Research
Naval Research Laboratory
Washington, DC 20375-5000

A. Wouters, S. Suckewer, E. Hinnov, and J.L. Schwob+
Princeton Plasma Physics Laboratory
Princeton University
Princeton, NJ 08544

August 1986

Submitted to the Journal of the Optical Society of America B.

ABSTRACT

High resolution spectra from the PLT plasma have been recorded by a 2 meter Schwob-Fraenkel soft X-ray multichannel spectrometer (SOXMOS). Spectra covering a wavelength range of approximately 50 Å were recorded every 50 ms, and the spectra were normalized and added together to produce composite spectra covering the region 80-340 Å. Several well-known reference lines were used to establish an absolute wavelength scale, and transition wavelengths were measured to an accuracy of approximately 0.02 Å. By subtracting spectra recorded at various times throughout the discharge, transitions from ions formed in the cooler and hotter plasmas were easily distinguished, and blends between hot and cold transitions were resolved. Wavelengths of transitions in C, O, Ti, Cr, Mn, Fe and Ni have been measured.

INTRODUCTION

The study of the soft X-ray spectroscopy of tokamak plasmas is important for the understanding of impurity concentrations, particle transport, and radiation losses (for a review, see Ref. 1). The H, He, and Li-like resonance transitions of the light impurities C and O and the $\Delta n=0$ ground state transitions of the highly-ionized metallic impurities such as Ti, Cr, Fe and Ni appear in the XUV spectral region. The spectra of elements that do not occur naturally in tokamak plasmas can be studied by injecting the elements using the laser blow-off technique.

The unambiguous identification of the transitions, particularly the transitions in the heavy ions, requires the observation of a number of lines from each ionization stage. The time dependence of the radiation is useful in distinguishing transitions in ions that occur over a range of electron temperature, and high spectral resolution is necessary to resolve blends of closely-spaced lines.

Suckewer and Hinnov[2] measured the intensities of a number of allowed transitions in the wavelength range 90-300 Å from Fe XVIII, Fe XX, and Fe XXII. Stratten et al.[3] observed $\Delta n=0$ transitions below 200 Å from Ti, Cr, Ni, and Ge with a spectral resolution of 0.7 Å.

In this paper, we present time-resolved spectra that were recorded by the 2 meter Schwob-Fraenkel soft X-ray multichannel spectrometer (SOXMOS) at the PLT tokamak.[4-8] These spectra represent significant improvements in spectral resolution and wavelength coverage. An accurate wavelength scale was

established using well-known reference lines and the geometry of the instrument. This accurate wavelength scale was essential for the identification of many of the transitions and also allowed the precise comparison of spectra recorded at various times during the same discharge and from different discharges. The signal-to-noise ratio was improved by adding a number of spectra, and many blends between transitions in ions that occur during the cooler and hotter periods of the discharge were resolved by subtracting spectra recorded during these periods.

We discuss in detail the establishment of the absolute wavelength scale over the wavelength region 80-340 Å. This includes the corrections for the distortions introduced by the flat multichannel plate detector, the non-linearities in the optical fiber transmission lines, and the electronic noise. We present the spectra of the intrinsic elements C, O, Ti, Cr, Fe and Ni. The spectra of the elements injected by the laser blow-off technique will be presented in a separate paper.

EXPERIMENTAL DETAILS

The PLT tokamak produces plasmas with central electron densities up to 1×10^{14} cm^{-3} and central electron temperatures up to 2.5 keV in Ohmically heated discharges. The plasmas typically have durations of somewhat less than 1 sec.

The plasma was viewed radially by a 2 meter grazing incidence spectrometer.[4] The spectrometer was fitted with a 600 l/mm grating, and the wavelength coverage was 5-340 Å for a grating blazed at 1^{o} 31′ or 20-340 Å for

a grating blazed at 3^{o} 39'. The spectra were recorded by either one or two flat MgF_2-coated microchannel plates (MCP) that were interferometrically adjusted to be tangent to the Rowland circle. Each MCP is fitted with a phosphor screen image intensifier and coupled by a flexible fiber optic conduit to a 1024 element photodiode array. The photodiode array was controlled and read out by an optical multichannel analyzer. Each MCP was capable of covering a wavelength range of 20 Å at short wavelengths or up to 70 Å at the long wavelength limit. High spectral resolution and relatively low background was achieved over the entire wavelength range. The widths of isolated spectral lines were typically 0.2 Å at 20 Å and 0.3 Å at 300 Å.

Spectral scans were recorded at intervals of 50 msec throughout the PLT discharge. Typically 10 usable scans with strong spectral lines were obtained on each discharge. Spectral lines from ions that are formed at low electron temperatures appear intense in the first few scans of a discharge. These cold lines diminish as the Ohmic heating proceeds. During the following plateau regime, when the electron temperature and density are approximately constant, the hot lines are much more intense than the cold lines.

DATA REDUCTION

A typical example of the data recorded during the plateau regime is shown in Fig. 1(a). The MCP detector was positioned to record data between 210 Å and 222 Å, and shown in Fig. 1(a) are the counts recorded by pixels number 500 through 700 of the detector array. Superimposed on the spectral data is a periodic noise pattern that originates in the electronic components of the photodiode array detector. The period of the noise pattern for the wavelength

region of Fig. 1 is 4 pixels, and this corresponds to a wavelength range of 0.1 to 0.3 Å depending on the wavelength region. Since the period of the noise pattern is comparable to the width of the spectral lines, it is not possible to smooth out the noise pattern without spoiling the spectral resolution. The data recorded after the end of the discharge are pure noise, and the noise pattern recorded on adjacent scans during this time does not change in pixel position. Shown in Fig. 1(b) is the spectrum that remained after the noise pattern was subtracted from the data of Fig. 1(a). The differences between Fig. 1(a) and (b) are significant, and the subtraction of the noise pattern is essential for the establishment of an accurate wavelength scale.

The wavelength scale can be determined from the well-known relation

$$\lambda = d\,(\cos\alpha - \cos\beta) \qquad (1)$$

where λ is the wavelength, d^{-1} is the number of lines per unit length of grating, α is the angle of incidence, β is the angle of diffraction, and β_o is the angular position of the MCP pixel that is tangent to the Rowland circle. A detailed description of the experimental geometry is given in the Appendix (see Fig. A-1).

The wavelengths for the well-known standard lines that were obtained from the above equation were initially found to be slightly different from the accepted values. Two different factors contributed to the sizable errors in the measured wavelengths. The fiber optic taper between the MCP and the detector introduced a nonlinear dispersion in pixel position that increases as

a function of distance from the tangential pixel. Secondly, the measured values of the angular position β_0 of the tangential pixel were not very accurate.

To correct for these discrepancies, a calibration curve for pixel position was obtained in the following manner. For each experimental run, the pixel positions of the standard lines were measured by fitting Gaussian profiles. The expected pixel positions of the lines were calculated from the known wavelengths (see Appendix), and the differences between the measured and expected pixel positions were graphed as a function of pixel position as shown in Fig. 2. Such a calibration curve was generated for each MCP position. The angular positions β_0 were adjusted slightly from the experimentally measured values so that the calibration curves for each MCP position had the same shape. A final calibration curve was obtained by fitting a least-squares polynomial, and this calibration curve is characteristic of the MCP and the fiber optic taper and is independent of the MCP position. The calibration curve and the adjusted values of β_0 were then used to establish the wavelength scale for each MCP position. The accuracy of this wavelength scale is estimated to be 0.01 Å.

Since the MCP is flat and does not conform to the Rowland circle, the angular position β of the pixels is a non-linear function of position on the MCP. The angular coverage of each pixel also varies across the MCP, and this means that the spectral resolution in the data recorded at the two ends of the MCP is different. This is a consideration when overlapping spectra recorded at adjacent MCP positions are pieced together to form a composite spectrum that covers a wide wavelength range. In order to correct for this effect, the

pixel bin positions were numerically transformed to be linear in ξ, and the angular width $\Delta\xi$ of each bin was set equal to the original width of the tangential pixel. The counts were distributed into the new pixel bins based on the original angular widths of the pixels. As a result, the spectrum on one side of the tangential pixel was slightly stretched, and the spectrum on the other side was slightly compressed. The overlapping spectra from adjacent MCP positions can be aligned to an accuracy of 0.01 Å.

RESULTS

The spectra are shown in Figs. 3-8. The first order spectrum is indicated by the solid line, and the first order spectrum shifted to second and third order wavelengths is indicated by the dotted and dash lines, respectively. The strong spectral lines appeared in multiple orders, and these lines provided a good independent check on the absolute wavelength scale.

Listed in Table I are the measured wavelengths and the classifications of the transitions. The overall accuracy of the measured wavelengths is estimated to be 0.02 Å. Also listed in Table I are previously measured or calculated wavelengths from Refs. 9-16.

A number of lines are unidentified in Table I. From the time dependence of the intensities of these lines, it could be determined that an unknown transition was from an ion that was abundant early in the discharge or during the plateau regime, and these lines are labeled cold line (C.L.) or hot line (H.L.), respectively.

CONCLUSIONS

Numerical techniques were developed to analyze the spectral data from the 2 meter Schwob-Fraenkel spectrometer fitted with a flat MCP. Using reference spectral lines, the positions of the MCP were precisely determined, and corrections were made for the various non-linearities in the recorded data. Using a pixel calibration curve, a wavelength scale was established with an accuracy of 0.01 Å, and the wavelengths of the spectral features were measured to an overall accuracy of 0.02 Å. A large number of ground-state transitions in Ti, Cr, Mn, Fe, and Ni were identified.

REFERENCES

1. S. Suckewer, "Spectroscopic diagnostics of tokamak plasmas", Phys. Script. 23, 72 (1981).

2. S. Suckewer and E. Hinnov, "Iron forbidden lines in tokamak discharges", Phys. Rev. A 20, 578 (1979).

3. B.C. Stratton, H.W. Moss, S. Suckewer, U. Feldman, J.F. Seely, and A.K. Bhatia, "Relative intensities of $2s^2 2p^k - 2s 2p^{k+1}$ transitions in F I- to B I-like Ti, Cr, Fe, Ni, and Ge in a tokamak plasma: A comparison of experiment and theory", Phys. Rev. A 31, 2534 (1985).

4. A.S. Filler, J.L. Schwob, and B.S. Fraenkal, Proc. 5th Int. Conf. on UV Radiation Physics, Castex, M. Pouey and N. Pouey, Editors, CNRS Paris, Vol. 1, p. 86 (1977).

5. J.L. Schwob, A. Wouters, S. Suckewer, and M. Finkenthal, "Time-resolving multichannel soft X-ray spectrometer for tokamak plasma diagnositcs", Bull. Am. Phys. Soc. 28, 1252 (1983).

6. J.L. Schwob, A. Wouters, ~~and~~ S. Suckewer, F.P. Boody, and M. Finkenthal, "Time-resolved spectra in the 5-300 Å region emitted from the PLT and TFTR tokamak plasmas", Proc. 8th Int. Coll. on EUV and X-ray Spectroscopy of Astrophysical and Laboratory Plasmas, IAU Coll. No. 86 (1984).

7. A.W. Wouters, J.L. Schwob, F.P. Boody, and S. Suckewer, "Impurity radiation in TFTR in the 5-300 Å spectral region using a high resolution multichannel spectrometer", Bull. Am. Phys. Soc. 29, 1303 (1984).

8. J.H. Davé, U. Feldman, J.F. Seely, A. Wouters, E. Hinnov, and S. Suckewer, "Time-resolved Spectra in the 80-330 Å wavelength region from PLT tokamak plasmas", Rev. Sci. Instr. ~~(in press)~~ 57, 2053 (1986).

9. B. Edlén, "Comparison of theoretical and experimental level values of the

n=2 complex in ions isoelectronic with Li, Be, C, and F", Phys. Scr. 28, 51 (1983).

10. B. Edlén, "Comparison of theoretical and experimental level values of the n=2 configuration in the boron I isoelectronic sequence", Phys. Scr. 28, 483 (1983).

11. B. Edlén, "Comparison of theoretical and experimental level values of the n=2 configuration in the carbon I isoelectronic sequence", Phys. Scr. 31, 345 (1985).

12. B. Edlén, "Comparison of theoretical and experimental level values of the n=2 configurations in the nitrogen I isoelectronic sequence", Phys. Scr. 30, 135 (1984).

13. W.E. Behring, L. Cohen, U. Feldman, and G.A. Doschek, "The solar spectrum: Wavelengths and identifications from 160 to 770 angstroms", Ap. J. 203, 521 (1976).

14. W.L. Wiese, "Spectroscopic Data for Iron", NBS, Washington, DC, Published by Controlled Fusion Data Center (1985).

15. R.L. Kelly and L.J. Palumbo, "Atomic and Ionic Emission Lines Below 2000 Angstroms" NRL Report 7599, Washington (1973).

16. E. Hinnov (independent measurements), 1986.

APPENDIX

The geometry of the MCP, the fiber optic, and the detector is shown in Fig. A-1. Point P_0 on the MCP is tangent to the Rowland circle, and this point corresponds to pixel number p_0 on the detector. The arbitrary point P_1 on the MCP corresponds to pixel number p_1. If M is the magnification of the fiber optic and N is the number of pixels per unit length on the detector, then the distance between points P_0 and P_1 on the MCP is

$$A = (p_1 - p_0)M/N. \tag{A-1}$$

From the right triangle GOC,

$$B = R \sin \beta_0 \tag{A-2}$$

where B is half the distance from the center of the grating to the tangential point of the MCP, β_0 is the angular position of the tangential point, and R is the radius of the Rowland circle. Applying the Law of Sines to triangle GP_1P_0,

$$A/\sin(\delta\beta) = 2B/\sin(\pi - \beta_0 - \delta\beta) \tag{A-3}$$

where $\delta\beta = \beta_0 - \beta$ is the angular position of point P_1 measured from the tangential point P_0. Solving Eq. (A-3) for β and using Eqs. (A-1) and (A-2),

$$\beta = \beta_0 \pm \cot^{-1} \frac{[2RN/(p_0 - p_1)M - \cot\beta_0]}{[\cot\beta_0 - 2RN/(p_1 - p_0)M]} \quad \text{for } p_1 < p_0 \tag{A-4}$$

$$\beta = \beta_0 + \cot^{-1}[2RN/(p_1 - p_0)M + \cot\beta_0] \quad \text{for } p_1 > p_0 \tag{A-5}$$

~~for $p_1 > p_0$ and a similar expression for $p_1 < p_0$.~~

For each MCP position, a calibration curve similar to Fig. 2 was generated. The expected pixel positions of the standard lines were calculated from Eqs. (A-4) and (1) using the experimental values of the angular positions ζ_0 of the MCP. Small adjustments to the ζ_0 values were made so that the data points from all of the MCP positions fell on the same smooth curve. The adjustments to ζ_0 were within the experimental uncertainties in the measured positions of the MCP. A polynomial function was fitted to the data points as shown in Fig. 2, and this calibration curve was used to measure the wavelengths of the unknown lines.

FIGURE CAPTIONS

Fig. 1. The spectral data as a function of pixel position covering the wavelength region 210 - 222 Å. The unprocessed data is shown in (a), and the electronic background noise has been removed in (b).

Fig. 2. The calibration curve for the MCP. The ordinate is the difference between the expected and the measured pixel positions of the reference spectral lines, and the abscissa is the difference between the measured and the tangential pixel positions.

Fig. 3. The PLT spectrum for 80-120 Å.

Fig. 4. The PLT spectrum for 110-160 Å.

Fig. 5. The PLT spectrum for 155-205 Å.

Fig. 6. The PLT spectrum for 200-250 Å.

Fig. 7. The PLT spectrum for 245-295 Å.

Fig. 8. The PLT spectrum for 290-340 Å.

Fig. A-1. The geometry of the spectrometer showing the grating G and the flat microchannel plate MCP. The angle of incidence is α. The angular position of the point on the microchannel plate that is tangent to the Rowland circle is β_0, and p_0 is the pixel corresponding to the

tangential point p_0. The distance to arbitrary point p_1 is A, and ϕ is the angle of diffraction at this point.

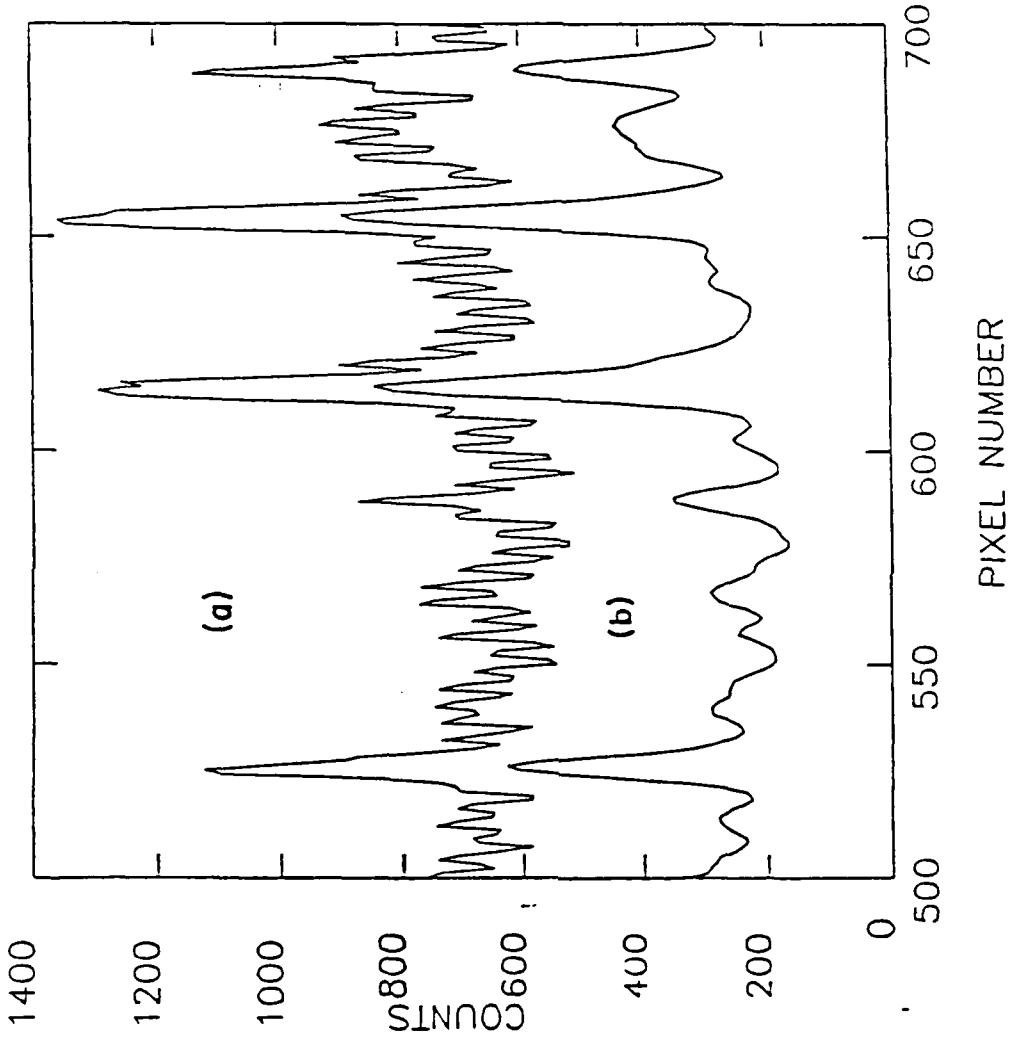
1400
1200
1000
800
600
400
200
0
COUNTS
500
550
600
650
700
PIXEL NUMBER
(a)
(b)

Fig. 1

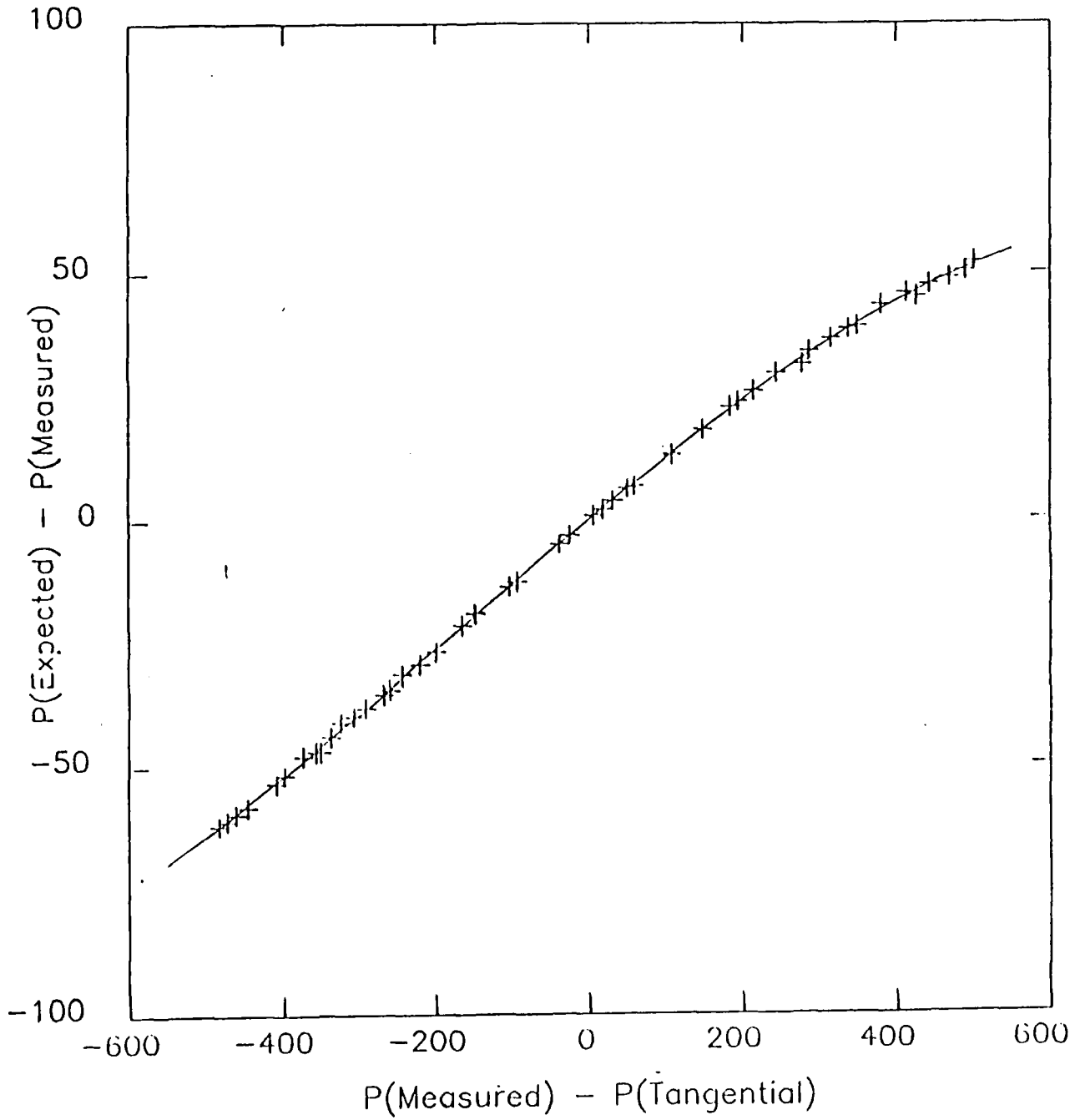
100
50
0
−50
−100
−600
−400
−200
0
200
400
600
P(Expected) − P(Measured)
P(Measured) − P(Tangential)

Fig 2

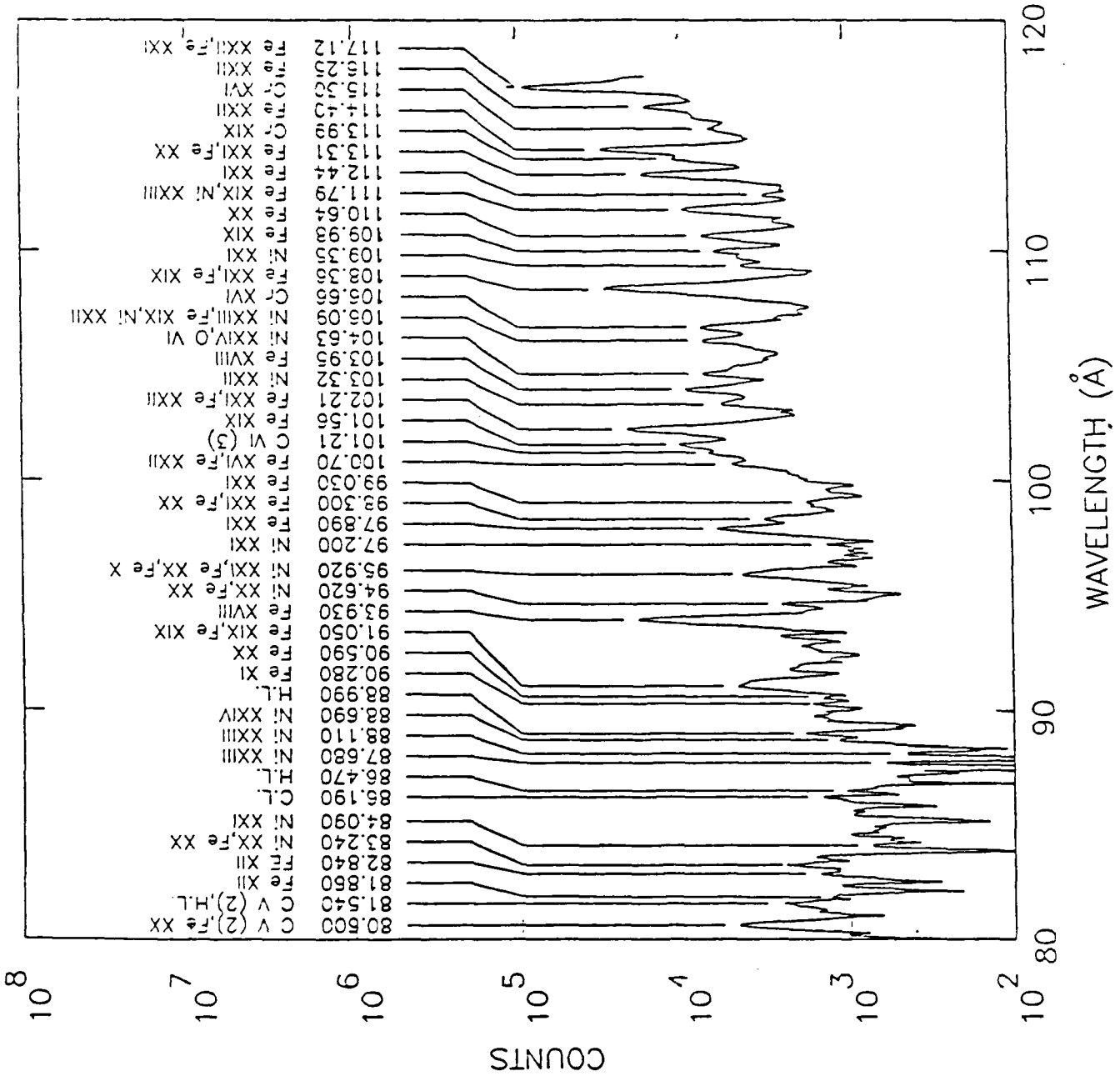
COUNTS
WAVELENGTH (Å)
80.600 C V (2),Fe XX
81.540 C V (2),H.L.
81.860 Fe XII
82.840 FE XII
83.240 Ni XX,Fe XX
84.090 Ni XXI
86.190 C.L.
86.470 H.L.
87.680 Ni XXIII
88.110 Ni XXIII
88.690 Ni XXIV
88.990 H.L.
90.280 Fe XI
90.590 Fe XX
91.050 Fe XIX,Fe XIX
93.930 Fe XVIII
94.620 Ni XX,Fe XX
95.920 Ni XXI,Fe XX,Fe X
97.200 Ni XXI
97.890 Fe XXI
93.300 Fe XXI,Fe XX
99.030 Fe XXI
100.70 Fe XVI,Fe XXII
101.21 C VI (3)
101.56 Fe XIX
102.21 Fe XXI,Fe XXII
103.32 Ni XXII
103.95 Fe XVIII
104.63 Ni XXIV,O VI
105.09 Ni XXIII,Fe XIX,Ni XXII
105.65 Cr XVI
108.36 Fe XXI,Fe XIX
109.35 Ni XXI
109.93 Fe XIX
110.64 Fe XX
111.79 Fe XIX,Ni XXIII
112.44 Fe XXI
113.31 Fe XXI,Fe XX
113.99 Cr XIX
114.40 Fe XXII
115.50 Cr XVI
116.25 Fe XXII
117.12 Fe XXII,Fe XXI

Fig. 3

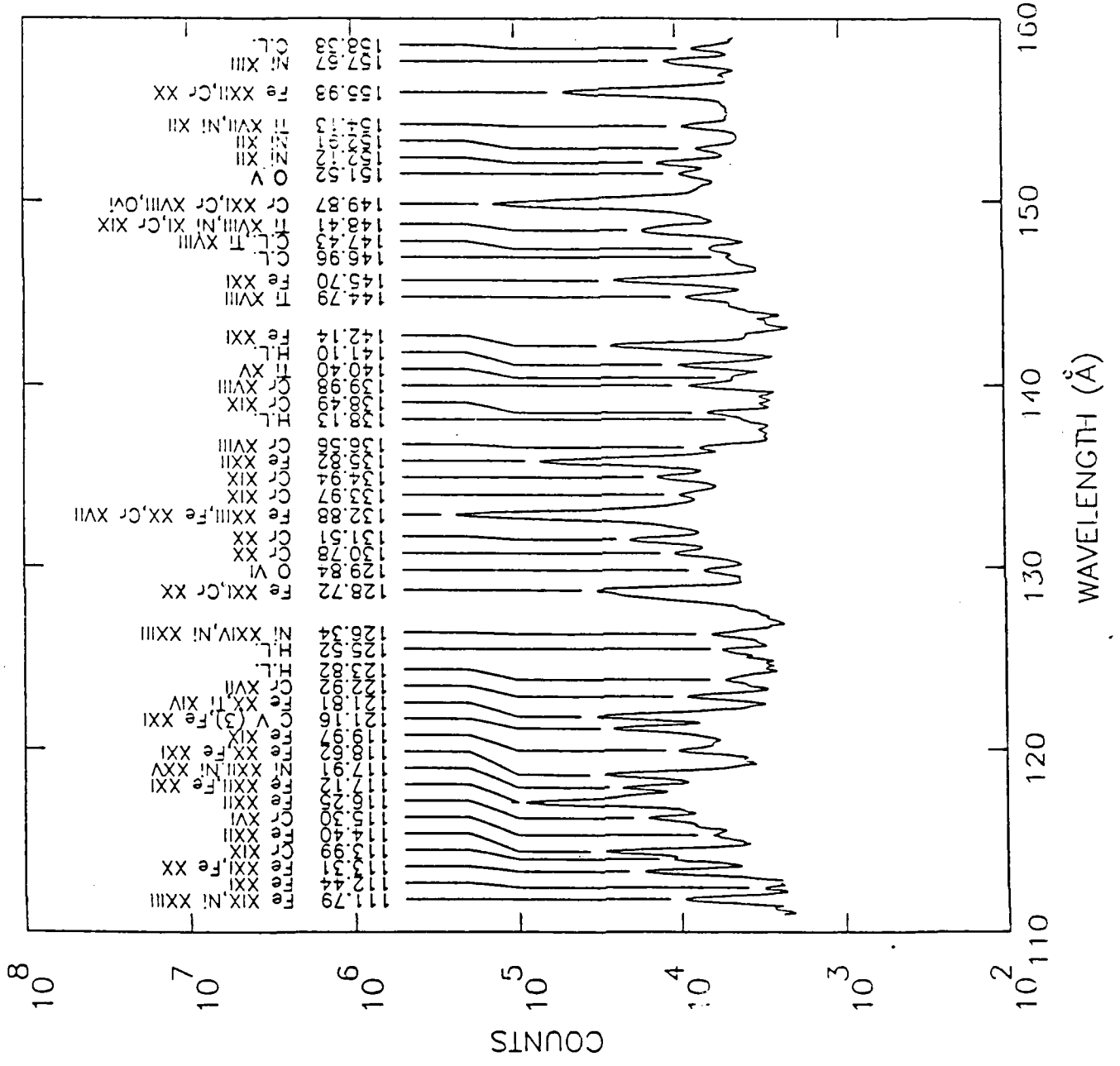
COUNTS
WAVELENGTH (Å)
111.79 Ni XXIV,Ni XXIII
112.44 Fe XXI
113.31 Fe XXI
113.99 Fe XIX,Fe XX
114.40 Fe XXII
114.53 Fe XVI
115.25 Fe XXII
117.12 Fe XXII,Fe XXI
117.91 Fe XXII,Ni XXIV
118.62 Fe XX,Fe XXI
119.97 Fe XIX
121.16 Fe V (3),Fe XXI
122.81 XX,Ti XIV
122.92 Fe XVII
123.82 H I (L)
125.52 H I (L)
126.34 Ni XXIV,Ni XXIII
128.72 Fe XXI,Cr XX
129.84 Fe VI
130.78 Fe Cr XX
131.51 Fe Cr XX
132.88 Fe XXIII,Fe XX,Cr XVII
133.97 Fe Cr XIX
134.94 Fe Cr XIX
135.82 Fe Cr XXII
136.56 Fe Cr XVIII
137.13 Fe Cr XIX
138.49 Fe Cr XVIII
139.98 Fe Cr XV
140.40 Fe XV
141.10 H I (L)
142.14 Fe XXI
144.79 Fe XVIII
145.70 Fe XXI
146.96 O I (L)
147.43 Fe XVIII
148.41 Fe XVIII,Ni XI,Cr XIX
149.87 Cr XXI,Cr XVIII,OVI
151.52 O V
152.27 Fe XII
153.03 Fe XVII,Ni XII
155.93 Fe XXII,Cr XX
157.67 Ni XIII
158.38 O I (L)

Fig. 4

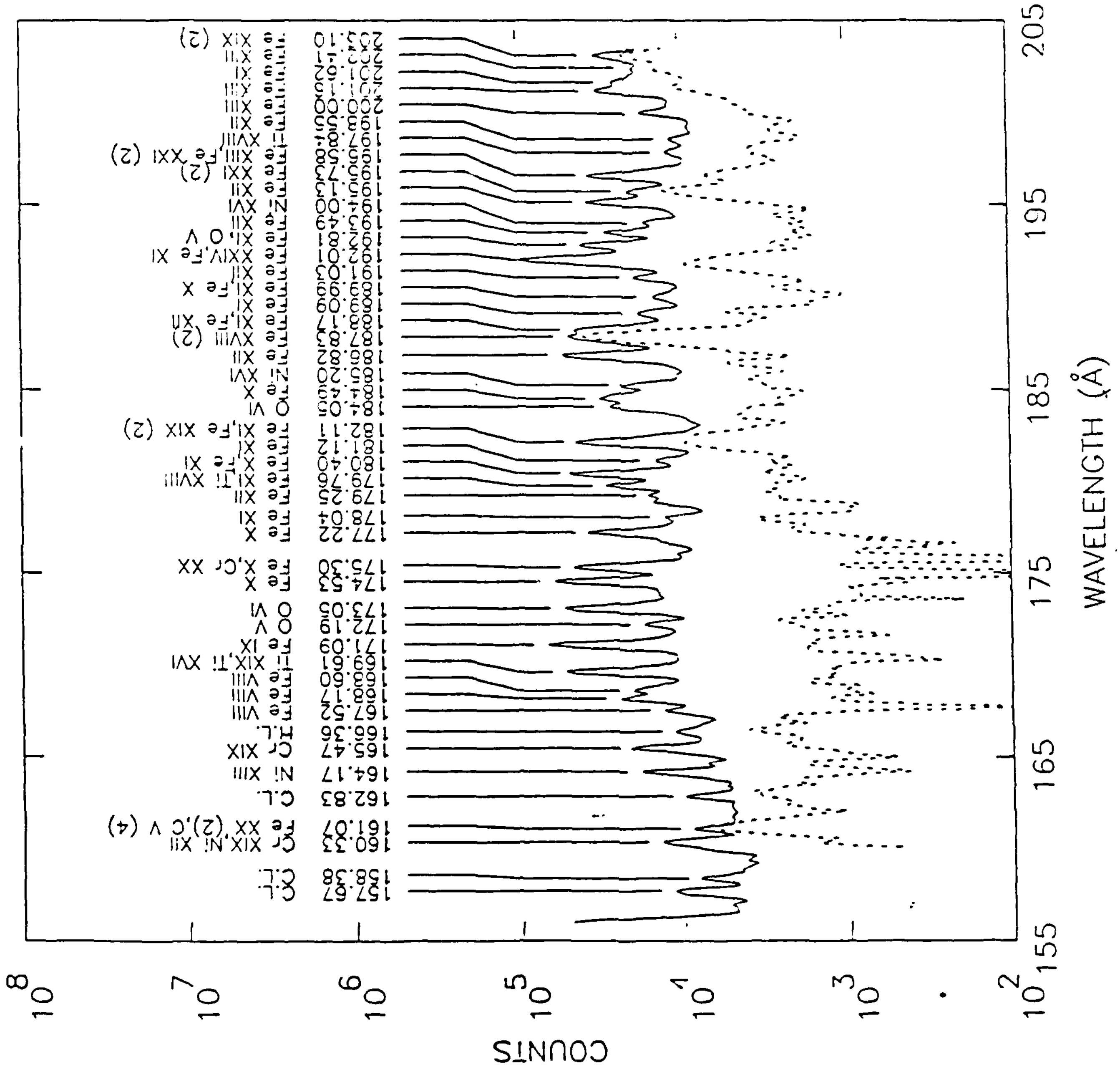

Fig. 5

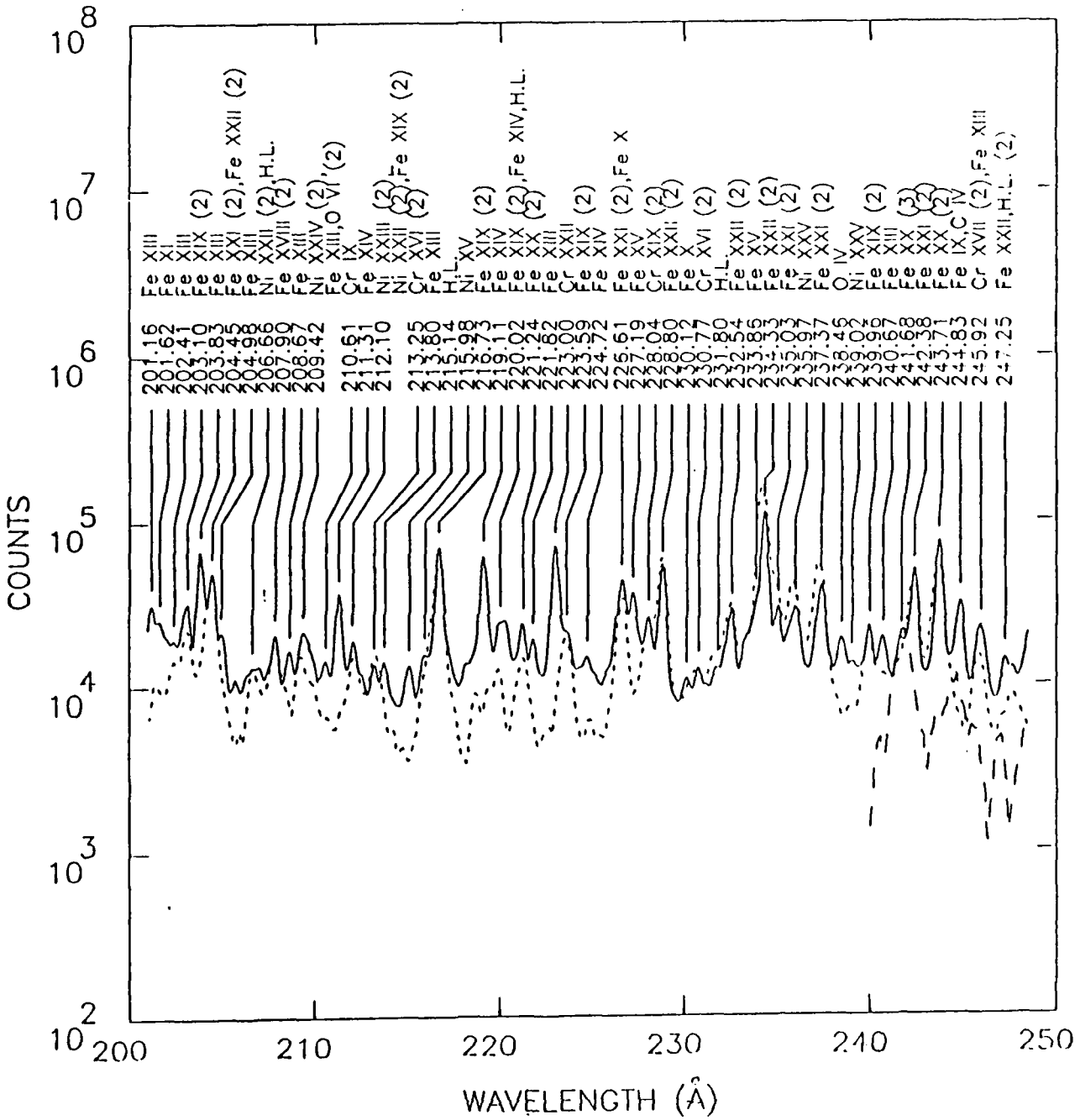
COUNTS
WAVELENGTH (Å)
200
210
220
230
240
250
10^2
10^3
10^4
10^5
10^6
10^7
10^8

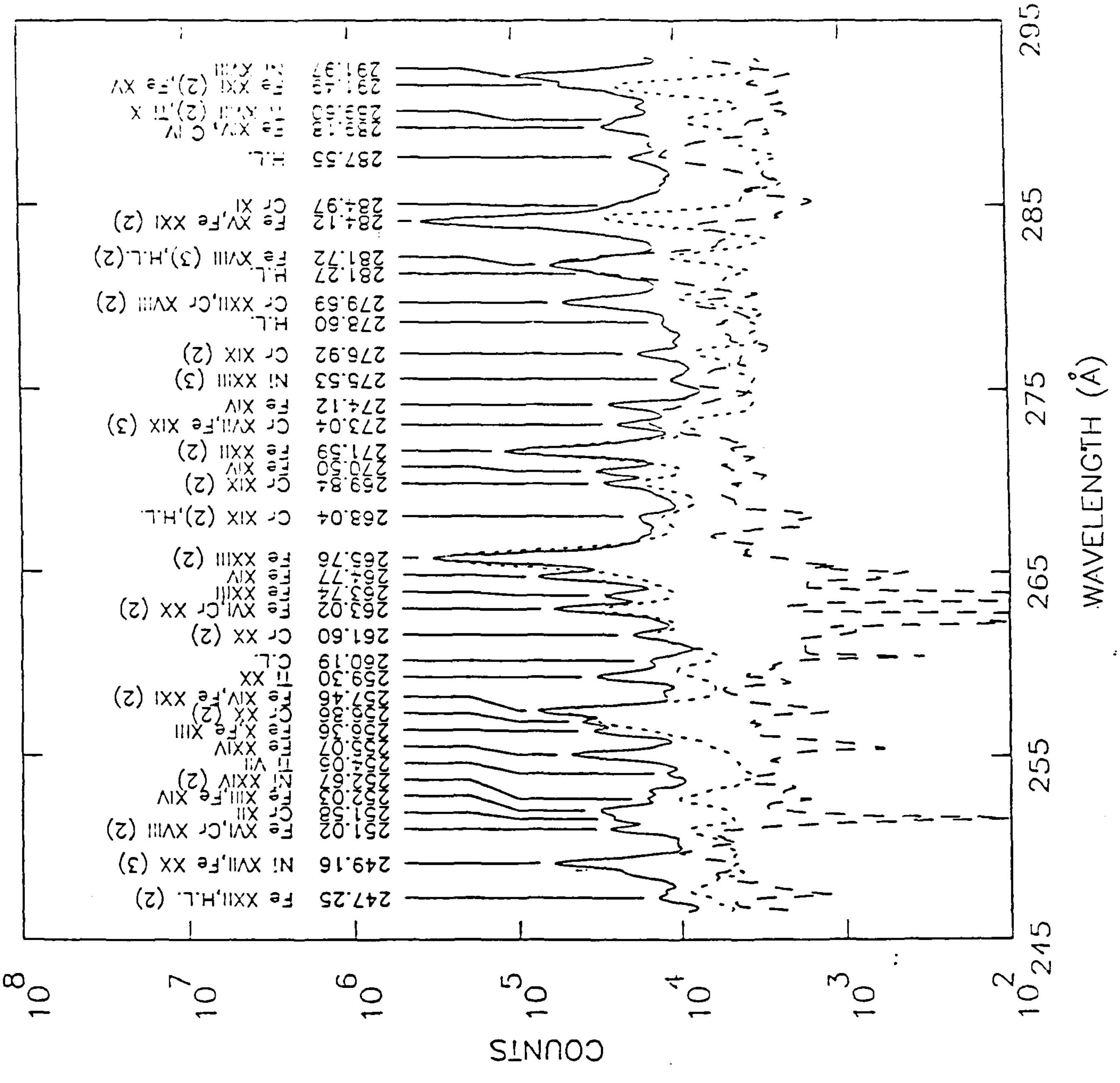
COUNTS
WAVELENGTH (Å)
245
255
265
275
285
295
247.25 Fe XXII,H.L. (2)
249.16 Ni XVII,Fe XX (3)
251.02 Fe XVI,Cr XVIII (2)
260.19 C.L.
261.60 Cr XX (2)
263.02 Fe XVI,Cr XX (2)
265.76 Fe XXIII (2)
268.04 Cr XIX (2),H.L.
269.84 Cr XIX (2)
271.59 Fe XXII (2)
273.04 Cr XVII,Fe XIX (3)
274.12 Fe XIV
275.53 Ni XXIII (3)
276.92 Cr XIX (2)
278.60 H.L.
279.69 Cr XXII,Cr XVIII (2)
281.27 H.L.
281.72 Fe XVIII (3),H.L.(2)
284.12 Fe XV,Fe XXI (2)
284.97 Cr XI
287.55 H.L.

Fig. 7

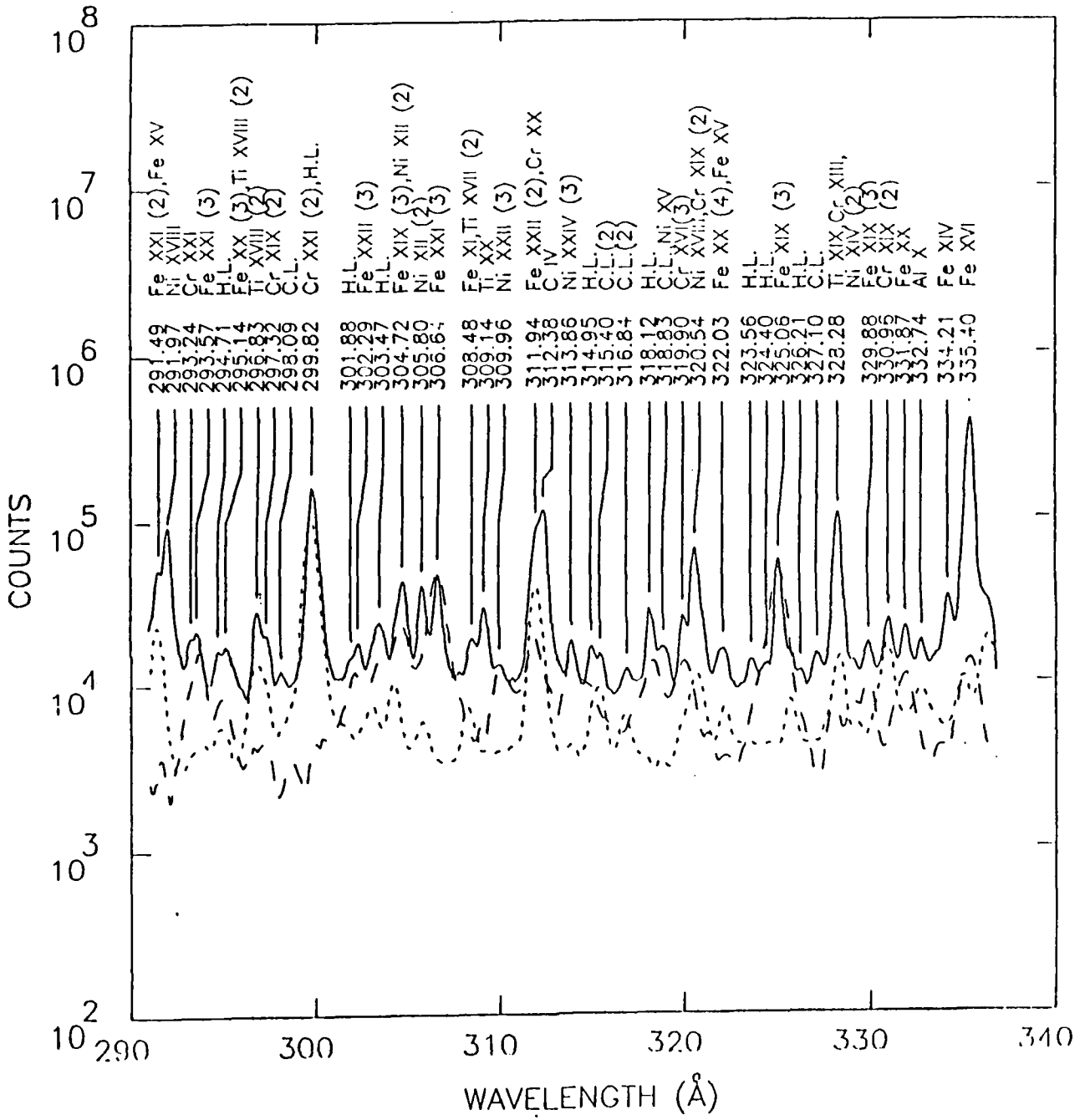
COUNTS
WAVELENGTH (Å)
290
300
310
320
330
340
Fe XXI (2),Fe XV
Ni XVIII
Cr XXI
Fe XXI (3)
H.L.
Fe XX (3),Ti XVIII (2)
Ti XVIII (2)
Cr XIX (2)
C.L.
Cr XXI (2),H.L.
H.L.
Fe XXII (3)
H.L.
Fe XIX (3),Ni XII (2)
Ni XII (2)
Fe XXI (3)
Fe XI,Ti XVII (2)
Ti XX
Ni XXII (3)
Fe XXII (2),Cr XX
C IV
Ni XXIV (3)
H.L.(2)
C.L.(2)
H.L.
Cr XVI(3),Ni XV
Ni XVII,Cr XIX (2)
Fe XX (4),Fe XV
H.L.
H.L.
Fe XIX (3)
H.L.
C.L.
Ti XIX,Cr XIII,
Ni XIV (2)
Fe XIX (3)
Cr XIX
Fe XX (2)
Al X
Fe XIV
Fe XVI
291.49
291.97
293.24
293.57
294.71
295.14
296.83
297.32
298.09
299.82
301.88
302.29
303.47
304.72
305.80
306.6
308.48
309.14
309.96
311.94
312.38
313.86
314.95
315.40
316.84
318.12
319.83
320.54
322.03
323.56
324.40
325.06
326.21
327.10
328.28
329.88
330.96
331.87
332.74
334.21
335.40

Fig. 8

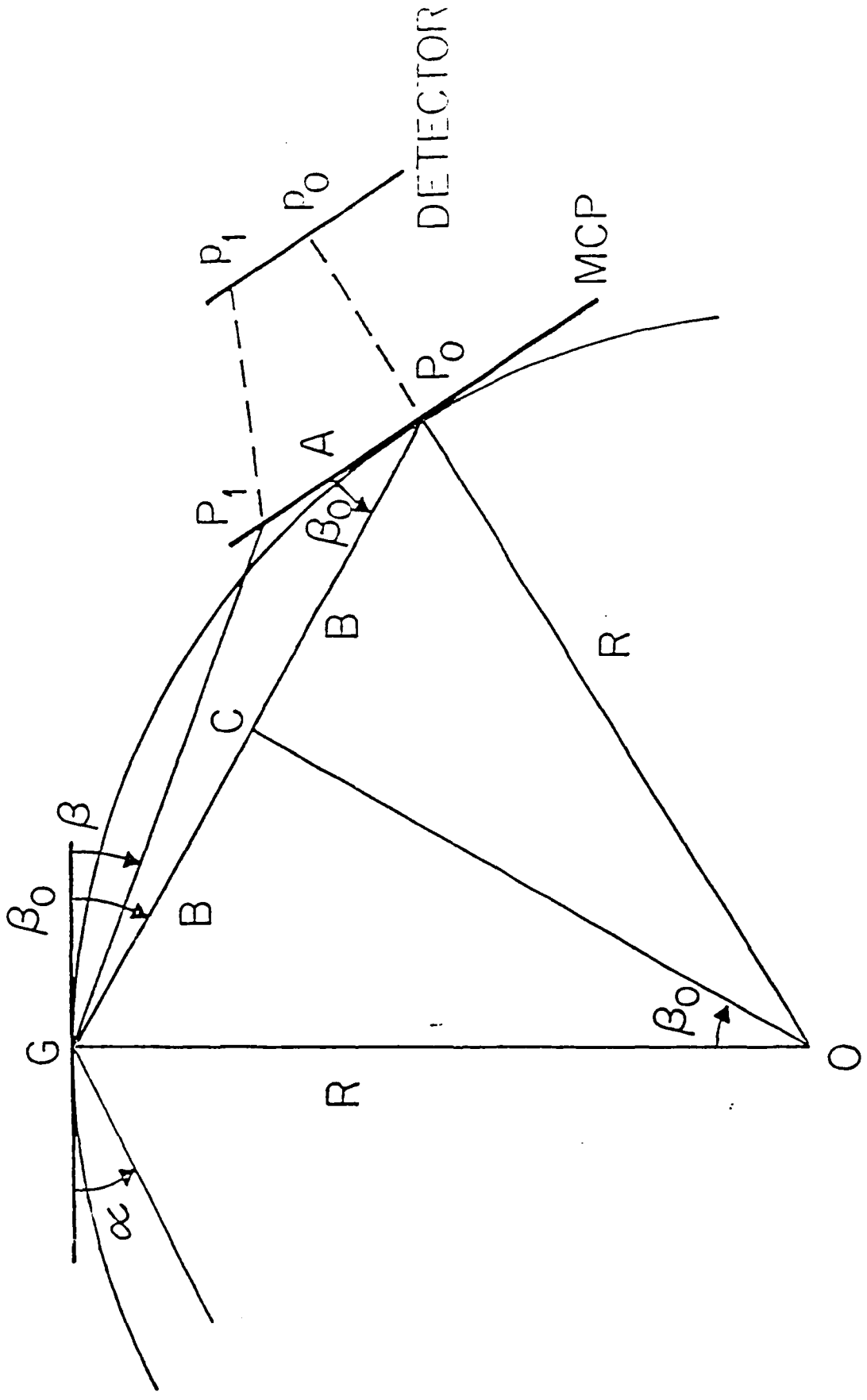
DETECTOR
MCP
P_0
P_1
P_0
P_1
A
β_0
B
C
B
R
β
β_0
G
R
β_0
O
α

Fig. A-1

TABLE I. Wavelengths and Transitions 80 Å - 340 Å

Wavelength (Å) Present	Previous[a]	Ion	Transition
80.17	80.23	Fe XII	$3p^3\ ^2D_{3/2} - 3p^2(^1D)4s\ ^2D_{5/2}$
80.60	40.27(2)	C V	$1s^2\ ^1S_0 - 1s2p\ ^1P_1$
	80.49	Fe XX	$2s^22p^3\ ^4S_{3/2} - 2s2p^4\ ^2P_{3/2}$
81.18		H.L	
81.47	40.73(2)	C V	$1s^2\ ^1S_0 - 1s2p\ ^3P_1$
81.54		H.L	
81.86bl	81.65	Fe XII	$3p^3\ ^2D_{3/2} - 3p^2(^3P)4s\ ^2P_{3/2}$
	81.94	Fe XII	$3p^3\ ^2D_{5/2} - 3p^2(^3P)4s\ ^2P_{3/2}$
82.32bl		C.L.	
82.84	82.84	Fe XII	$3p^3\ ^2P_{3/2} - 3p^2(^1D)4s\ ^2D_{5/2}$
83.24	83.18	Ni XX	$2s^22p^5\ ^2P_{3/2} - 2s2p^6\ ^2S_{1/2}$
	83.23	Fe XX	$2s^22p^3\ ^2D_{3/2} - 2s2p^4\ ^2P_{1/2}$
83.58		H.L.	
84.09bl	84.07	Ni XXII	$2s^22p^3\ ^2D_{5/2} - 2s2p^4\ ^2P_{3/2}$
84.57bl		H.L.	
85.59bl		H.L.	
86.19		C.L.	
86.47		C.L.	
87.68	87.67	Ni XXIII	$2s^22p^2\ ^3P_1 - 2s2p^3\ ^3S_1$
88.11	88.11	Ni XXIII	$2s^22p^2\ ^1D_2 - 2s2p^3\ ^1P_1$
88.69bl	88.61	Ni XXIV	$2s^22p\ ^2P_{1/2} - 2s2p^2\ ^2P_{3/2}$
88.99		H.L.	
89.73		H.L.	

90.28b1	90.21	Fe XI	$3p^4\ ^3P_1 - 3p^3(^4S)4s\ ^3S_1$
90.59b1	90.61	Fe XX	$2s^2 2p^3\ ^2D_{3/2} - 2s2p^4\ ^2P_{3/2}$
91.05	91.02	Fe XIX	$2s^2 2p^4\ ^1D_2 - 2s2p^5\ ^1P_1$
91.27b1	91.27	Fe XXI	$2s^2 2p^2\ ^3P_0 - 2s2p^3\ ^3S_1$
91.84b1	91.87	Ni XXIII	$2s^2 2p^2\ ^3P_2 - 2s2p^3\ ^3S_1$
92.79		H.L.	
93.22		C.L.	
93.93	93.93	Fe XVIII	$2s^2 2p^5\ ^2P_{3/2} - 2s2p^6\ ^2S_{1/2}$
94.62	94.50	Ni XX	$2s^2 2p^5\ ^2P_{1/2} - 2s2p^6\ ^2S_{1/2}$
	94.64	Fe XX	$2s^2 2p^3\ ^2D_{3/2} - 2s2p^4\ ^2S_{1/2}$
95.25		H.L.	
95.92	95.86	NI XXI	$2s^2 2p^4\ ^3P_2 - 2s2p^5\ ^3P_2$
	95.92	Fe XX	$2s^2 2p^3\ ^4S_{3/2} - 2s2p^4\ ^2D_{3/2}$
96.12b1	96.12	Fe X	$3p^5\ ^2P_{3/2} - 3p^4(^3P)4s\ ^2P_{3/2}$
96.45		H.L.	
96.77	96.80	Ni XXI	$2s^2 2p^4\ ^3P_0 - 2s2p^5\ ^3P_1$
97.20	97.15	Ni XXI	$2s^2 2p^4\ ^1S_0 - 2s2p^5\ ^1P_1$
97.89b1	97.86	Fe XXI	$2s^2 2p^2\ ^3P_1 - 2s2p^3\ ^3S_1$
98.30	98.36	Fe XXI	$2s^2 2p^2\ ^1D_2 - 2s2p^3\ ^1P_1$
	98.35	Fe XX	$2s^2 2p^3\ ^2P_{3/2} - 2s2p^4\ ^2P_{1/2}$
99.03	99.02	Fe XXI	$2s^2 2p^2\ ^3P_2 - 2s2p^3\ ^1D_2$
100.25b1	100.24	Ni XXI	$2s^2 2p^4\ ^3P_1 - 2s2p^5\ ^3P_1$
100.70b1	50.35(2)	Fe XVI	$2p^6 3s\ ^2S_{1/2} - 2p^6 4p\ ^2P_{3/2}$
	100.77	Fe XXII	$2s^2 2p\ ^2P_{1/2} - 2s2p^2\ ^2P_{3/2}$
101.21	33.73(3)	C VI	$1s\ ^2S_{1/2} - 2p\ ^2P_{1/2}$
	33.74(3)	C VI	$1s\ ^2S_{1/2} - 2p\ ^2P_{3/2}$
101.56	101.56	Fe XIX	$2s^2 2p^4\ ^3P_2 - 2s2p^5\ ^3P_1$

102.21	102.21	Fe XXI	$2s^2 2p^2\ ^3P_2 - 2s2p^3\ ^3S_1$
	102.22	Fe XXII	$2s^2 2p\ ^2P_{1/2} - 2s2p^2\ ^2P_{1/2}$
	102.10	Ni XXIV	$2s^2 2p\ ^2P_{3/2} - 2s2p^2\ ^2P_{3/2}$
103.32	103.31	Ni XXII	$2s^2 2p^3\ ^4S_{1/2} - 2s2p^4\ ^4P_{1/2}$
103.95	103.94	Fe XVIII	$2s^2 2p^5\ ^2P_{1/2} - 2s2p^6\ ^2S_{1/2}$
104.63	104.63	Ni XXIV	$2s^2 2p\ ^2P_{1/2} - 2s2p^2\ ^2S_{1/2}$
104.81b1	104.81	O VI	$2s\ ^2S_{1/2} - 5p\ ^2P_{3/2}$
106.09	106.05	Ni XXIII	$2s^2 2p^2\ ^3P_2 - 2s2p^3\ ^3P_2$
	106.05	Ni XXII	$2s^2 2p^3\ ^4S_{3/2} - 2s2p^4\ ^4P_{3/2}$
	106.11	Fe XIX	$2s^2 2p^4\ ^1S_0 - 2s2p^5\ ^1P_1$
106.32b1	106.32	Fe XIX	$2s^2 2p^4\ ^3P_1 - 2s2p^5\ ^3P_0$
106.66	106.63	Cr XVI	$2s^2 2p^5\ ^2P_{3/2} - 2s2p^6\ ^2S_{1/2}$
108.11b1	108.11	Fe XXI	$2s^2 2p^2\ ^3P_0 - 2s2p^3\ ^3P_1$
108.36	108.36	Fe XIX	$2s^2 2p^4\ ^3P_2 - 2s2p^5\ ^3P_2$
109.35	109.31	Ni XXI	$2s^2 2p^4\ ^3P_1 - 2s^2 2p^5\ ^3P_2$
109.73		H.L.	
109.98	109.95	Fe XIX	$2s^2 2p^4\ ^3P_0 - 2s2p^5\ ^3P_1$
110.64	110.63	Fe XX	$2s^2 2p^3\ ^2D_{3/2} - 2s2p^4\ ^2D_{3/2}$
111.79	111.70	Fe XIX	$2s^2 2p^4\ ^3P_1 - 2s2p^5\ ^3P_1$
	111.83	Ni XXIII	$2s^2 2p^2\ ^3P_0 - 2s2p^3\ ^3D_1$
112.44	112.45	Fe XXI	$2s^2 2p^2\ ^1S_0 - 2s2p^3\ ^1P_1$
113.31	113.29	Fe XXI	$2s^2 2p^2\ ^1D_2 - 2s2p^3\ ^1D_2$
	113.35	Fe XX	$2s^2 2p^3\ ^2D_{5/2} - 2s2p^4\ ^2D_{5/2}$
113.99b1	114.01	Cr XIX	$2s^2 2p^2\ ^3P_2 - 2s2p^3\ ^3S_1$
114.40	114.41	Fe XXII	$2s^2 2p\ ^2P_{3/2} - 2s2p^2\ ^2P_{3/2}$
115.30	115.36	Cr XVI	$2s^2 2p^5\ ^2P_{1/2} - 2s2p^6\ ^2S_{1/2}$
115.82	115.82	O VI	$2s\ ^2S_{1/2} - 4p\ ^2P_{3/2}$

	115.83	O VI	$2s\ ^2S_{1/2} - 4p\ ^2P_{1/2}$
116.25	116.27	Fe XXII	$2s^2 2p\ ^2P_{3/2} - 2s2p^2\ ^2P_{1/2}$
117.12	117.18	Fe XXII	$2s^2 2p\ ^2P_{1/2} - 2s2p^2\ ^2S_{1/2}$
117.49b1	117.49	Fe XXI	$2s^2 2p^2\ ^3P_1 - 2s2p^3\ ^3P_1$
117.91	117.92	Ni XXII	$2s^2 2p^3\ ^4S_{3/2} - 2s2p^4\ ^4P_{5/2}$
	117.94[b]	Ni XXV	$2s^2\ ^1S_0 - 2s2p\ ^1P_1$
	118.47	Ni XXIV	$2s^2 2p\ ^2P_{1/2} - 2s2p^2\ ^2D_{3/2}$
118.62	118.68	Fe XX	$2s^2 2p^3\ ^4S_{3/2} - 2s2p^4\ ^4P_{1/2}$
	118.69	Fe XXI	$2s^2 2p^2\ ^3P_1 - 2s2p^3\ ^3P_0$
119.97	119.99	Fe XIX	$2s^2 2p^4\ ^3P_1 - 2s2p^5\ ^3P_2$
120.35	120.35	Ni XXI	$2s^2 2p^4\ ^1D_2 - 2s2p^5\ ^3P_2$
120.81b1	40.27(3)	C V	
121.16	121.19	Fe XXI	$2s^2 2p^2\ ^3P_2 - 2s2p^3\ ^3P_2$
121.81	121.85	Fe XX	$2s^2 2p^3\ ^4S_{3/2} - 2s2p^4\ ^4P_{3/2}$
	121.99	Ti XIV	$2s^2 2p^5\ ^2P_{3/2} - 2s2p^6\ ^2S_{1/2}$
122.92	122.97	Cr XVII	$2s^2 2p^4\ ^3P_2 - 2s2p^5\ ^3P_2$
123.82		H.L.	
125.52	125.52	Cr XVIII	$2s^2 2p^3\ ^2D_{3/2} - 2s2p^4\ ^2D_{3/2}$
126.34	126.30	Ni XXIV	$2s^2 2p\ ^2P_{3/2} - 2s2p^2\ ^2S_{1/2}$
126.59b1	126.59	Ni XXIII	$2s^2 2p^2\ ^3P_1 - 2s2p^3\ ^3D_2$
128.44b1	128.44	Cr XX	$2s^2 2p\ ^2P_{3/2} - 2s2p^2\ ^2P_{3/2}$
128.72	128.73	Fe XXI	$2s^2 2p^2\ ^3P_0 - 2s2p^3\ ^3D_1$
129.84	129.79	O VI	$2p\ ^2P_{1/2} - 4d\ ^2D_{3/2}$
	129.87	O VI	$2p\ 2P_{3/2} - 4d\ ^2D_{5/2}$
130.78	130.75	Cr XX	$2s^2 2p\ ^2P_{3/2} - 2s2p^2\ ^2P_{1/2}$
131.51	131.57	Cr XX	$2s^2 2p\ ^2P_{1/2} - 2s2p^2\ ^2S_{1/2}$
132.88[c]	132.88	Fe XXIII	$2s^2\ ^1S_0 - 2s2p\ ^1P_1$

PAGES 5, 8

ARE

MISSING

IN

ORIGINAL

DOCUMENT

151.52	151.5	O V	$2s2p\ ^3P - 2s4d\ ^3D$
152.12	152.15	Ni XII	$3p^5\ ^2P_{3/2} - 3p^4(^3P)3d\ ^2D_{5/2}$
152.91	152.94	Ni XII	$3p^5\ ^2P_{1/2} - 3p^4(^3P)3d\ ^2P_{3/2}$
154.13	154.13	Ti XVII	$2s^22p^2\ ^3P_1 - 2s2p^3\ ^3P_0$
	154.17	Ni XII	$3p^5\ ^2P_{3/2} - 3p^4(^3P)3d\ ^2P_{3/2}$
155.98	155.94	Fe XXII	$2s^22p\ ^2P_{3/2} - 2s2p^2\ ^2D_{5/2}$
	155.98	Cr XX	$2s^22p\ ^2P_{1/2} - 2s2p^2\ ^2D_{3/2}$
157.67	157.73	Ni XIII	$3s^23p^4\ ^3P_2 - 3s^23p^33d\ ^3D_3$
158.38		C.L.	
159.97b1	159.97	Ni XII	$3p^5\ ^2P_{1/2} - 3p^4(^3P)\ ^2P_{3/2}$
160.33	160.32	Cr XIX	$2s^22p^2\ ^3P_1 - 2s2p^3\ ^3D_2$
161.07	80.49(2)	Fe XX	
	40.27(4)	C V	
162.83		C.L.	
164.17	164.15	Ni XIII	$3s^23p^4\ ^3P_2 - 3s^23p^33d\ ^3P_2$
165.47	165.46	Cr XIX	$2s^22p^2\ ^3P_2 - 2s2p^3\ ^3D_3$
166.36		H.L.	
167.52	167.49	Fe VIII	$3p^63d\ ^2D_{3/2} - 3p^5(3d^2(^3F))\ ^2D_{3/2}$
168.17	168.17	Fe VIII	$3p^63d\ ^2D_{5/2} - 3p^5(3d^2(^3F))\ ^2D_{5/2}$
168.60	168.55	Fe VIII	$3p^63d\ ^2D_{5/2} - 3p5(3d^2(^3P))\ ^2P_{3/2}$
169.61	169.58	Ti XIX	$2s^2\ ^1S_0 - 2s2p\ ^1P_1$
169.74b1	169.74	Ti XVI	$2s^2\ 2p^3\ ^4S_{3/2} - 2s\ 2p^4\ ^4P_{5/2}$
171.09	171.07	Fe IX	$3p^6\ ^1S_0 - 3p^53d\ ^1P_1$
172.19	172.17	O V	$2s^2\ ^1S_0 - 2s3p\ ^1P_1$
173.05	172.94	O VI	$2p\ ^2P_{1/2} - 3d\ ^2D_{3/2}$
	173.08	O VI	$2p\ ^2P_{3/2} - 3d\ ^2D_{3/2}$
174.53	174.53	Fe X	$3p^5\ ^2P_{3/2} - 3p^4(^3P)3d\ ^3D_{5/2}$

175.26	Fe X	$3p^5\ ^2P_{1/2} - 3p^4(^3P)3d\ ^2D_{3/2}$
175.36	Cr XX	$2s^22p\ ^2P_{3/2} - 2s2p^2\ ^2D_{5/2}$
	H.L.	
177.24	Fe X	$3p^5\ ^2P_{3/2} - 2p^4(^3P)3d\ ^2P_{3/2}$
178.06	Fe XI	$3p^4\ ^3P_2 - 3p^3(^4S)3d\ ^3D_2$
	C.L.	
179.27	Fe XII	$3p^3\ ^2D_{5/2} - 3p^2(^3P)3d\ ^2D_{5/2}$
179.76	Fe XI	$3p^4\ ^1D_2 - 3p^3(^2D)3d\ ^1F_3$
179.90	Ti XVIII	$2s^22p\ ^2P_{1/2} - 2s2p^2\ ^2D_{3/2}$
180.45	Fe X	$3p^5\ ^2P_{1/2} - 3p^43d(^3P)\ ^2P_{1/2}$
180.40	Fe XI	$3p^4\ ^3P_2 - 3p^3(^4S)3d\ ^3D_3$
181.14	Fe XI	$3p^4\ ^3P_0 - 3p^3(^4S)3d\ ^3D_1$
91.02(2)	Fe XIX	
182.17	Fe XI	$3p^4\ ^3P_1 - 3p^3(^4S)3d\ ^3D_2$
91.27(2)	Fe XXI(2)	
183.94	O VI	$2p\ ^2P_{1/2} - 3s\ ^2S_{1/2}$
184.12	O VI	$2p\ ^2P_{3/2} - 3s\ ^2S_{1/2}$
184.54	Fe X	$3p^5\ ^2P_{3/2} - 3p^4(^1D)3d\ ^2S_{1/2}$
185.23	Ni XVI	$3p\ ^2P_{1/2} - 3d\ ^2D_{3/2}$
186.86	Fe XII	$3p^3\ ^2D_{3/2} - 3p^2(^3P)3d\ ^2F_{5/2}$
186.88	Fe XII	$3p^3\ ^2D_{5/2} - 3p^2(^3P)3d\ ^2F_{7/2}$
93.93(2)	Fe XVIII	
188.17	Fe XII	$3p^3\ ^2P_{1/2} - 3p^2(^3P)3d\ ^2D_{3/2}$
188.22	Fe XI	$3p^4\ ^3P_2 - 3p^3(^2D)3d\ ^3P_2$
189.13	Fe XI	$3p^4\ ^3P_1 - 3p^3(^2D)3d\ ^3P_1$
189.94	Fe XI	$3p^4\ ^3P_2 - 3p^3(2_D)3d\ ^1P_1$
190.04	Fe X	$3p^5\ ^2P_{1/2} - 3p^4(^1D)3d\ ^2S_{1/2}$

207.90	103.94(2)	Fe XVIII	
208.67	208.68	Fe XIII	$3p^2\ ^1S_0 - 3p3d\ ^1P_1$
209.42bl	104.63(2)	Ni XXIV	
	209.62	Fe XIII	$3p^2\ ^3P_1 - 3p3d\ ^3P_2$
	104.81(2)	O VI	
209.92bl	209.92	Fe XIII	$3p^2\ ^3P_2 - 3p3d\ ^3P_1$
210.61	210.62	Cr IX	$3p^4\ ^3P_2 - 3p^3(^4S)3d\ ^3D_3$
211.31	211.32	Fe XIV	$3p\ ^2P_{1/2} - 3d\ ^2D_{3/2}$
212.10	106.05(2)	Ni XXIII	
	106.05(2)	Ni XXII	
	106.11(2)	Fe XIX	
212.50bl		H.L.	
213.25	106.63(2)	Cr XVI	
213.80	213.77	Fe XIII	$3p^2\ ^3P_2 - 3p3d\ ^3P_2$
215.14		H.L.	
215.98	215.94	Ni XV	$3s^23p^2\ ^3P_1 - 3s3p^3\ ^3S_1$
216.73	108.36(2)	Fe XIX	
218.26		C.L.	
219.11	219.12	Fe XIV	$3p\ ^2P_{3/2} - 3d\ ^2D_{5/2}$
220.02bl	109.95(2)	Fe XIX	
	220.08	Fe XIV	$3p\ ^2P_{3/2} - 3d\ ^2D_{3/2}$
220.29bl		H.L.	
221.24	110.63(2)	Fe XX	
221.82	221.82	Fe XIII	$3p^2\ ^1D_2 - 3p3d\ ^1D_2$
223.00	223.01	Cr XXII	$2s\ ^2S_{1/2} - 2p\ ^2P_{3/2}$
223.59	111.70(2)	Fe XIX	
224.72	224.75	Fe XV	$3p3d\ ^3P_0 - 3s3d\ ^3D_1$

226.30b1	226.30	Fe X	$3p^5\ ^2P_{3/2} - 3p^4(^1D)3d\ ^2D_{5/2}$
226.61	113.29(2)	Fe XXI	
227.19	227.21	Fe XV	$3s3p\ ^3P_1 - 3s3d\ ^3D_2$
	227.2	O V, C V	
228.04	114.01(2)	Cr XIX	
228.80	114.41(2)	Fe XXII	
230.12	230.09	Fe X	$3p^5\ ^2P_{3/2} - 3p^4(^1D)3d\ ^2D_{3/2}$
230.77	115.36(2)	Cr XVI	
231.80b1		H.L.	
232.54	116.27(2)	Fe XXII	
233.32b1		H.L.	
233.86b1	233.86	Fe XV	$3s3p\ ^3P_2 - 3s3d\ ^3D_3$
234.33	117.18(2)	Fe XXII	
235.03	117.49(2)	Fe XXI	
235.97b1	117.94(2)[b]	Ni XXV	
237.37	118.69(2)	Fe XXI	
238.46	238.36	O IV	$2p\ ^2P_{1/2} - 3d\ ^2D_{3/2}$
	238.57	O IV	$2p\ ^2P_{3/2} - 3d\ ^2D_{5/2}$
239.02	238.86	Ni XXV	$2s^2\ ^1S_0 - 2s2p\ ^3P_1$
239.96	119.99(2)	Fe XIX	
240.67	240.71	Fe XIII	$3s^23p^2\ ^3P_0 - 3s3p^3\ ^3S_1$
241.68	80.49(3)	Fe XX	
242.38	121.19(2)	Fe XXI	
243.71	121.85(2)	Fe XX	
244.83	244.91	Fe IX	$3p^6\ ^1S_0 - 3p^53d\ ^3P_1$
	244.91	C IV	$2s\ ^2S_{1/2} - 4p\ ^2P_{3/2}$
245.92	122.97(2)	Cr XVII	

246.21bl	246.21	Fe XIII	$3s^2 3p^2\ ^3P_1 - 3p^3 3d\ ^3S_1$
247.25	247.20	Fe XXII	$2s^2 2p\ ^2P_{1/2} - 2s 2p^2\ ^4P_{1/2}$
247.65	123.82(2)	H.L.	
248.52		C.L.	
249.16	249.18	NI XVII	$3s^2\ ^1S_0 - 3s 3p\ ^1P_1$
249.54bl	83.18(3)	Fe XX	
251.02	125.52(2)	Cr XVIII	
	251.07	Fe XVI	$3p\ ^2P_{1/2} - 3d\ ^2D_{3/2}$
251.58	251.52	Cr XII	$3p\ ^2P_{3/2} - 3d\ ^2D_{5/2}$
252.03	251.95	Fe XIII	$3s^2 3p^2\ ^3P_2 - 3s 3p^3\ ^3S_1$
	252.19	Fe XIV	$3s^2 3p\ ^2P_{1/2} - 3s 3p^2\ ^2P_{3/2}$
252.67	126.30(2)	Ni XXIV	
253.09		C.L.	
254.06bl	254.02	Ti VII	$3p^4\ ^3P_2 - 3p^3(^4S)3d\ ^3D_3$
255.07	255.08	Fe XXIV	$2s\ ^2S_{1/2} - 2p\ ^2P_{1/2}$
256.36	256.38	Fe X	$3p^5\ ^2P_{3/2} - 3p^4(^3P)3d\ ^4D_{3/2}$
	256.42	Fe XIII	$3s^2 3p^2\ ^1D_2 - 3s 3p^3\ ^1P_1$
256.86	128.42(2)	Cr XX	
257.46	257.39	Fe XIV	$3s^2 3p\ ^2P_{1/2} - 3s 3p^2\ ^2P_{1/2}$
	128.73(2)	Fe XXI	
259.30	259.29	Ti XX	$2s\ ^2S_{1/2} - 2p\ ^2P_{3/2}$
260.19		C.L.	
261.60	130.75(2)	Cr XX	
263.02	262.97	Fe XVI	$3p\ ^2P_{3/2} - 3d\ ^2D_{5/2}$
	131.57(2)	Cr XX	
263.74	263.74	Fe XXIII	$2s^2\ ^1S_0 - 2s 2p\ ^3P_1$
264.77	264.79	Fe XIV	$3s^2 3p\ ^2P_{3/2} - 3s 3p^2\ ^2P_{3/2}$

265.76	132.88(2)	Fe XXIII	
267.79bl		H.L.	
268.04bl	134.05(2)	Cr XIX	
269.84	134.94(2)	Cr XIX	
270.50	270.52	Fe XIV	$3s^2 2p\ ^2P_{3/2} - 3s3p^2\ ^2P_{1/2}$
271.59	135.76(2)	Fe XXII	
273.04	136.59(2)	Cr XVII	
	91.02(3)	Fe XIX	
274.12	274.20	Fe XIV	$3s^2 3p\ ^2P_{1/2} - 3s3p^2\ ^2S_{1/2}$
275.53bl	91.87(3)	Ni XXIII	
276.92	138.52(2)	Cr XIX	
278.60		H.L.	
279.69	279.72	Cr XXII	$2s\ ^2S_{1/2} - 2p\ ^2P_{1/2}$
	139.87(2)	Cr XVIII	
281.27bl		H.L.	
281.72	93.93(3)	Fe XVIII	
282.14bl	141.09(2)	Mn XXII	
283.64bl	283.64	Fe XII	$3s^2 3p^3\ ^2D_{3/2} - 3s3p^4\ ^2P_{1/2}$
284.12	284.15	Fe XV	$3s^2\ ^1S_0 - 3s3p\ ^1P_1$
284.28bl	142.14(2)	Fe XXI	
284.97bl	284.97	Cr XI	$3s^2 3p^2\ ^3P_1 - 3s3p^3\ ^3S_1$
287.55		H.L.	
289.18	289.16	Fe XIV	$3s^2 3p\ ^2P_{3/2} - 3s3p^2\ ^2S_{1/2}$
	289.2	C IV	$2p\ ^2P - 4d\ ^2D$
289.60bl	144.76(2)	Ti XVIII	
	289.58	Ti X	$3p\ ^2P_{1/2} - 3d\ ^2D_{3/2}$
290.33	290.31	Cr XI	$3s^2 3p^2\ ^3P_2 - 3s3p^3\ ^3S_1$

291.01bl	291.01	Fe XII	$3s^2 3p^3\ ^2D_{5/2} - 3s3p^4\ ^2P_{3/2}$
291.49	145.70(2)	Fe XXI	
291.97	292.00	Ni XVIII	$3s\ ^2S_{1/2} - 3p\ ^2P_{3/2}$
293.24bl	293.16	Cr XXI	$2s^2\ ^1S_0 - 2s2p\ ^3P_1$
293.57	97.86(3)	Fe XXI	
294.71bl		H.L.	
295.14bl	98.35(3)	Fe XX	
	147.56(2)	Ti XVIII	
295.58bl	295.58	Ti X	$3p\ ^2P_{3/2} - 3d\ ^2D_{5/2}$
296.83	148.46(2)	Ti XVIII	
297.32bl	148.66(2)	Cr XIX	
298.09	C.L.		
299.82	149.89(2)	Cr XXI	
300.27bl	150.12(2)	O VI	
301.88bl		H.L.	
302.29	100.77(3)	Fe XXII	
302.93bl	151.52(2)	O V	
303.47bl		H.L.	
304.32	152.15(2)	Ni XII	
304.72	101.56(3)	Fe XIX	
305.80	152.94(2)	Ni XII	
306.64	102.21(3)	Fe XXI	
308.48bl	154.13(2)	Ti XVII	
	308.54	Fe XI	$3s^2 3p^4\ ^1D_2 - 3s3p^5\ ^1P_1$
309.14	309.09	Ti XX	$2s\ ^2S_{1/2} - 2p\ ^2P_{1/2}$
309.96	103.31(3)	Ni XXII	
311.94bl	155.94(2)	Fe XXII	

	155.98(2)	Cr XX	
312.38	312.42	C IV	$2s\ ^2S_{3/2} - 3p\ ^2P_{3/2}$
	312.43	C IV	$2s\ ^2S_{1/2} - 3p\ ^2P_{1/2}$
313.86	104.63(3)	Ni XXIV	
314.95		H.L.	
315.40	157.67(2)	C.L.	
316.84	158.38(2)	C.L.	
318.12bl		H.L.	
318.83bl	318.67	C.L.	
	319.01	Ni XV	$3s^2 3p^2\ ^3P_2 - 3s 3p^3\ ^3D_3$
319.90	106.63(3)	Cr XVI	
320.54bl	320.55	Ni XVIII	$3s\ ^2S_{1/2} - 3p\ ^2P_{1/2}$
	160.32(2)	Cr XIX	
321.78bl	321.78	Fe XV	$3s 3p\ ^3P_2 - 3p^2\ ^3P_1$
322.03bl	80.49(4)	Fe XX	
323.56		H.L.	
324.40		H.L.	
325.06	108.36(3)	Fe XIX	
325.68	162.83(2)	C.L.	
326.21		H.L.	
327.10bl		C.L.	
328.28	328.34	Ti XIX	$2s^2\ ^1S_0 - 2s 2p\ ^3P_1$
	328.29	Cr XIII	$3s^2\ ^1S_0 - 3s 3p\ ^1P_1$
	164.15(2)	Ni XIV	
329.88	109.95(3)	Fe XIX	
330.96	165.46(2)	Cr XIX	$2s^2 2p^2\ ^3P_2 - 2s 2p^3\ ^3D_3$
331.87	110.63(3)	Fe XX	

332.74	332.77	Al X	$2s^2\ {}^1S_0 - 2s2p\ {}^1P_1$
334.21	334.17	Fe XIV	$3s^23p\ {}^2P_{1/2} - 3s3p^2\ {}^2D_{3/2}$
335.40	335.40	Fe XVI	$3s\ {}^2S_{1/2} - 3p\ {}^2P_{3/2}$

---

[a] The previously measured wavelengths are from Refs. 9-15.

[b] Independent measurement by E. Hinnov is 117.99 Å.

[c] Independent measurement by E. Hinnov is 132.913 Å.